Nanotechnology **24** (2013) 115301 (6pp) doi:10.1088/0957-4484/24/11/115301

Effect of using stencil masks made by focused ion beam milling on permalloy ($Ni_{81}Fe_{19}$) nanostructures

J R Bates[1], Y Miyahara[1], J A J Burgess[2,3], Ó Iglesias-Freire[4] and P Grütter[1]

[1] McGill University, Department of Physics Montreal, QC H3A 2T8, Canada
[2] Department of Physics, University of Alberta Edmonton, AB T6G 2G7, Canada
[3] National Institute of Nanotechnology Edmonton, AB T6G 2M9, Canada
[4] Instituto de Ciencia de Materiales de Madrid, CSIC Madrid, E-28049, Spain

E-mail: batesj@physics.mcgill.ca

Received 5 November 2012, in final form 7 January 2013
Published 28 February 2013
Online at stacks.iop.org/Nano/24/115301

Abstract
Focused ion beam (FIB) milling is a common fabrication technique to make nanostencil masks which has the unintended consequence of gallium ion implantation surrounding milled features in silicon nitride membranes. We observe major changes in film structure, chemical composition, and magnetic behaviour of permalloy nanostructures deposited by electron beam evaporation using silicon nitride stencil masks made by a FIB as compared to stencil masks made by regular lithography techniques. We characterize the stenciled structures and both types of masks using transmission electron microscopy, electron energy loss spectroscopy, energy dispersive x-ray spectroscopy, magnetic force microscopy and kelvin probe force microscopy. All these techniques demonstrate distinct differences at a length scale of a 1–100 nm for the structures made using stencil mask fabricated using a FIB. The origin of these differences seems to be related to the presence of implanted ions, a detailed understanding of the mechanism however remains to be developed.

(Some figures may appear in colour only in the online journal)

1. Introduction

The current standard techniques used for fabrication of sub-micron device features include electron beam lithography [1, 2], interferometric lithography [2, 3], extreme ultraviolet and x-ray lithography [2]. Nanostencil lithography can be advantageous over lift-off techniques in that resist coating, solvents and etching can be avoided [4, 5]. This reduces the number of possible contamination sources, with the added benefit of being able to prepare and analyse the sample while maintaining ultra-high vacuum (UHV) conditions. Stencil lithography can be used in static [6–9] or dynamic mode [10–13] and is used in a variety of different applications such as magnetic nanostructures [11, 14–16], fabrication of *in situ* interconnects [17, 18], molecular beam epitaxial deposition through a stencil mask [13, 19] and defining clean metal patterns [5, 7, 8, 20–22]. Nanostencils are commonly fabricated by focused ion beam (FIB) techniques [4, 23].

In this work, we demonstrate that FIB-milled nanostencils can lead to a substantial change in structure, chemical composition and magnetic behaviour of resulting nanostructures deposited by electron beam evaporation when compared to the permalloy ($Ni_{81}Fe_{19}$) starting material. We present a possible explanation attributing the changes in structure and magnetic behaviour to electric charge of gallium ions implanted in the mask surrounding milled features. The change in chemical composition, although correlated with FIB-milled nanostencils, is not presently understood.

2. Sample preparation

A dual column FIB and scanning electron microscope (FEI strata DB-235, 30 kV, 10 and 30 pA ion beam current with

 © 2013 IOP Publishing Ltd Printed in the UK & the USA

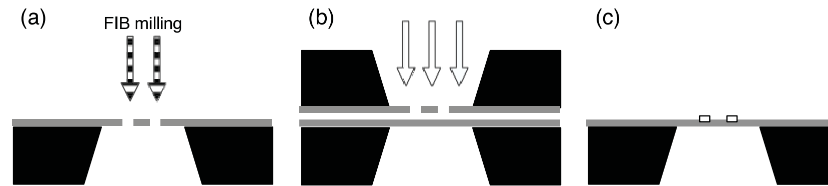

Figure 1. Sample preparation schematic (not to scale). Black, grey, white and striped represent silicon, silicon nitride, permalloy and gallium ions respectively. (a) A nanostencil mask is made by milling holes in a silicon nitride membrane using a FIB. (b) The nanostencil mask is placed on top of the SiN membrane and permalloy is evaporated through the holes. The gap is due to imperfections in the stencil and substrate such as dust particles or membrane warping. (c) The nanostencil is removed and permalloy nanostructures are left where the nanostencil holes were located.

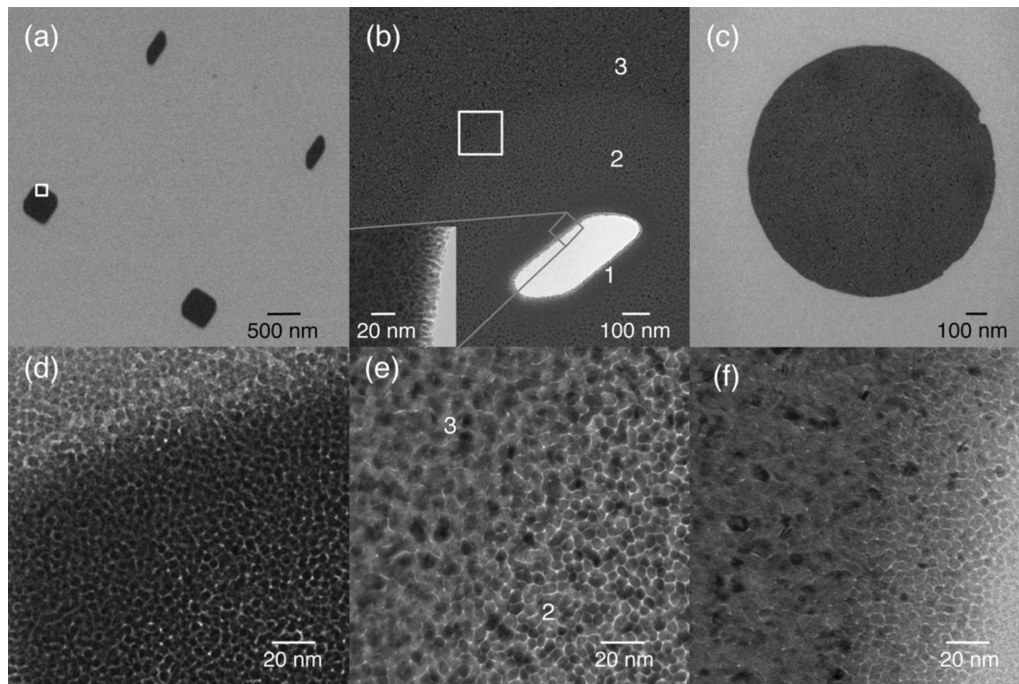

Figure 2. Bright field TEM images of: (a) permalloy nanostructures fabricated using the FIB nanostencil; (b) FIB-milled nanostencil used to make (a) after permalloy deposition, with permalloy film visible featuring two morphology zones surrounding the milled hole, the inset is a zoom in on the edge of the hole; (c) 1 μm diameter permalloy dot deposited through a stencil mask made by conventional photolithography; (d)–(f) higher resolution images of structures fabricated in the same way as (a)–(c) respectively.

dwell times of 12 and 4 s μm^{-2} respectively, base pressure of 5.5×10^{-7} mbar) was used to mill holes in a 100 nm thick SiN membrane (Norcada NT025C) that was covered on both sides with 10 nm of sputtered gold palladium ($Au_{60}Pd_{40}$ by weight) prior to FIB milling. Milling was done from the SiN side of the membrane (as shown in figure 1(a)), the ion column was used to mill the holes and the electron column was used to image the resulting holes. The membrane was then brought into contact with an uncoated SiN membrane and 20 nm of permalloy ($Ni_{81}Fe_{19}$) was evaporated using an electron beam evaporator (BJD 1800, deposition rate $\sim$1 Å s^{-1}, or an Omicron EFM3 electron beam evaporator, deposition rate $\sim$0.05 Å s^{-1}), as shown schematically in figure 1. All samples were exposed to air before characterization took place. A control sample was made using an uncoated SiN nanostencil that was created using conventional photolithography (PL) (Protochips DTM-25232, thickness 200 nm) instead of a FIB to compare the effects of the FIB milling. Samples made using the FIB-milled stencil and samples made using the PL stencil were made with both evaporators.

3. Results and discussion

A transmission electron microscope (TEM) (Philips CM200) was used to look at a FIB-milled nanostencil, the resulting nanostructures after permalloy deposition as well as at the sample made with the PL nanostencil, as seen in figure 2. The TEM images show that there is a difference between the permalloy growth in the deposited nanostructures made with the FIB stencil (figure 2(d)) and the permalloy growth in the nanostructure made with the PL stencil (figure 2(f)). Figure 2(d) shows columnar growth perpendicular to the film with gaps around each column, whereas figure 2(f) has more of an isotropic growth. The permalloy growth of the FIB nanostencil shows these two distinct growth modes (figures 2(b) and (e)). The morphology of the nanostructure

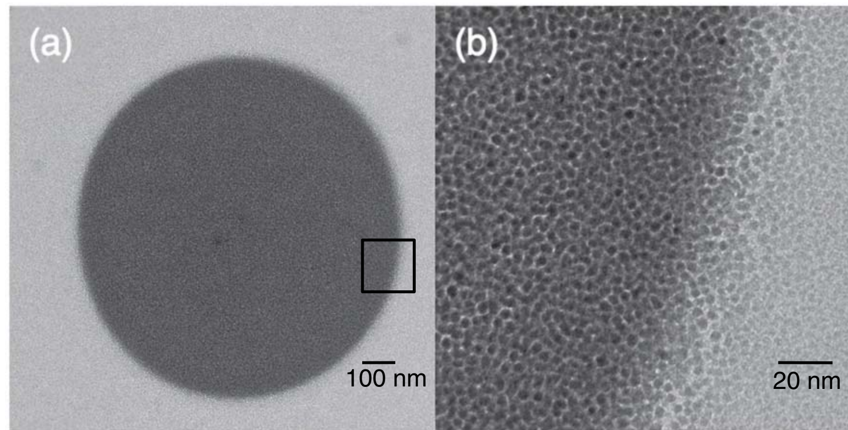

Figure 3. Bright field TEM images of (a) permalloy nanostructures 1 μm in diameter, fabricated using the FIB nanostencil; (b) zoom in on the edge of the black box shown in (a).

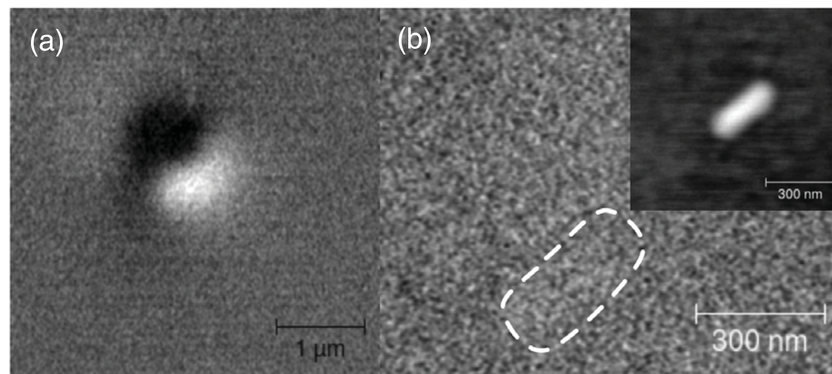

Figure 4. (a) MFM image of a 1 μm in diameter 20 nm thick permalloy nanostructure in a 48 kA m^{-1} in-plane magnetic field, lift height of 100 nm, colour scale 1.2 Hz, prepared using the stencil made by conventional photolithography. (b) MFM image of the permalloy nanostructure fabricated by the FIB milled nanostencil, 400 nm by 200 nm by 20 nm in a 48 kA m^{-1} in-plane magnetic field, lift height of 70 nm, colour scale 0.1 Hz. The inset is a non-contact atomic force microscope image of the nanostructure in (b), the z scale 25 nm.

made with the FIB stencil in figure 2(d) is very similar to the morphology of the deposited permalloy near the FIB stencil hole, as shown in figure 2(e) zone 2, both showing columnar growth with gaps around the columns. The morphology of the deposited permalloy made with the PL stencil in figure 2(f) is very similar to the morphology far from the FIB stencil hole, as shown in figure 2(e) zone 3, both showing a more isotropic growth. Figure 3 shows a 1 μm diameter structure made using a FIB-milled stencil that shows the same growth mode that is seen in figure 2(d). The structure from figure 3 was evaporated simultaneously in the same evaporator as the sample in figure 2(f). This confirms that the differences are not a result of a variation between different evaporation methods, evaporation runs or exposure to air, but due to differences in stencil masks as a result of FIB or PL based fabrication processes.

Magnetic force microscopy (MFM) [24–26] was then performed on both samples using a home built instrument to measure their magnetic properties. Using the same MFM cantilever (Smart Tip SC-35-M), the samples were scanned at a constant lift height varying from 30 to 100 nm in an in-plane external magnetic field of 48 kA m^{-1}. Clear MFM contrast is visible on the nanostructures made using a PL stencil (figure 4(a)), while none of the nanostructures made using a FIB-milled nanostencil (which range in size from 120 nm by 400 nm to 1 μm in diameter) showed magnetic contrast (figure 4(b)). This effect was observed repeatedly over many independent experiments and MFM cantilevers.

To understand what could be causing the differences in the properties and structure, electron energy loss spectroscopy (EELS) [27] measurements were made to determine the composition of the permalloy and oxygen content. There was a significant difference in composition; the samples made with the FIB stencil had no iron within measurement error whereas the sample made with the PL stencil had a composition of $Ni_{77\pm3}Fe_{23\pm3}$, which is close to the expected composition of the evaporant ($Ni_{81}Fe_{19}$). Although nickel has a lower saturation magnetization when compared to permalloy, it is not sufficiently low to explain the lack of MFM contrast. Nanostructures made using a FIB-milled

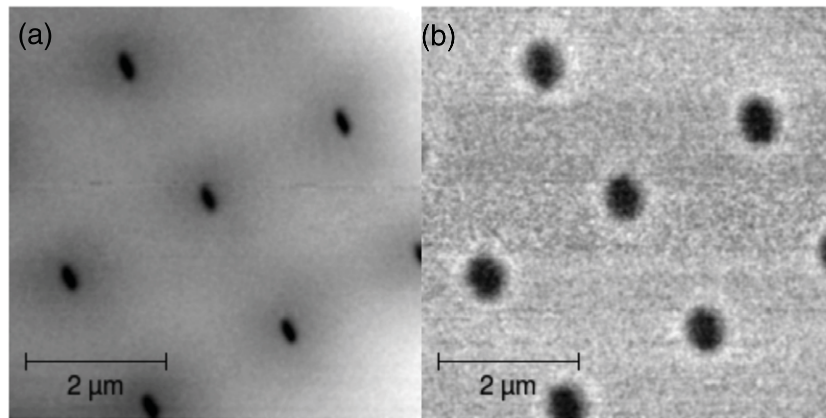

Figure 5. Simultaneously acquired (a) non-contact constant frequency shift topography and (b) Kelvin probe microscopy images of the FIB fabricated nanostencil. The image scale is 150 nm and 1 V for (a) and (b) respectively. Black represents positive charges and white represents negative charges in the Kelvin probe microscopy image.

stencil and a PL stencil were also analysed to look at oxygen content, as oxide has anti-ferromagnetic ordering which would result in an absence of MFM contrast. There was approximately three times the oxygen content in the nanostructures made with a FIB-milled stencil when compared to the nanostructures made with a PL stencil. The bare SiN substrate was also measured on each sample and was found to have the same oxygen content within experimental error, which suggests that the oxygen differences are not a result of differences in surface contamination or substrates. To confirm that gold palladium was not responsible for the adverse changes an additional sample was made using the same PL stencil coated with gold palladium. The resulting nanostructures had the same chemical composition as the bare PL stencil, with clearly visible contrast in MFM.

Electric fields are known to influence permalloy growth [28], and gallium ions have been shown to implant around FIB-milled features in silicon [29, 30]. Gallium ions were found surrounding FIB-milled holes using energy dispersive x-ray spectroscopy [31]. We propose that the electric field from the gallium ions in this system is perpendicular to the plane of film growth (in contrast to the work by Bochkarev *et al* [28]). Because electron beam evaporation is not a charge neutral process [32–34], we suggest that the presence of an electric field could affect the growth of charged permalloy species. The presence of an electric field may also induce polarization in growing islands during deposition and serve to encourage growth in the direction of the field lines (normal to the plane of the surface) through interaction with the polarized species deposited. This hypothesis is supported by the TEM data collected, which reveal that permalloy film grains surrounding FIB-milled nanostencil features, as well as those within nanostructures, appear circular, indicating cylindrical column growth out of the surface plane. The inset of figure 2(b) also supports the hypothesis as growth is seen to be perpendicular to the side of the milled holes that is parallel to the expected electric field at the edge of the hole. The cylindrical column growth is not seen far from the FIB-milled areas where there would be no gallium ions, as shown in figure 2(e) zone 3.

To verify the presence of an electric field in regions where gallium ion implantation takes place, Kelvin probe force microscopy was performed on a nanostencil mask [34, 35]. A variation of the surface potential can be observed in a circular area $1.1 \pm 0.2\ \mu$m in a diameter around the FIB-milled area, as shown in figure 5(b), approximately the same size as the area of zone 2 in figure 2(b). Positive gallium ions are attributed to the dark region in figure 5(b) while the white ring surrounding the hole is attributed to screening of gallium ions by electrons in the AuPd layer.

Selected area electron diffraction (SAED) images were then taken for each sample to get a quantitative measurement of the differences in growth (figure 6). Each SAED was radially averaged, the background subtracted and a Lorentzian function was fitted to the (1,1,1) peak. The sample made using a FIB stencil and the area on the stencil near the FIB-milled hole (figure 2(e) zone 2) had a FWHM of 0.070 ± 0.001 Å^{-1} and 0.067 ± 0.001 Å^{-1} respectively. In contrast, the FWHMs of the sample made with the PL stencil and the FIB-milled stencil far from the milled hole (figure 2(e) zone 3) are almost half the width at 0.034 ± 0.001 Å^{-1} and 0.038 ± 0.001 Å^{-1}, respectively. This increase in width of the (1,1,1) peak could be attributed to a decrease in grain size [31], or a result of NiO, which has peaks within 0.03 Å^{-1} on each side of the permalloy (1,1,1) peak. However, the increased oxygen content measured from EELS in the FIB-milled stencil indicates that the broadening seen in the SAED of the permalloy (1,1,1) peak is due to NiO, which also explains the absence of signal in MFM as NiO is anti-ferromagnetic. Oxidization of nickel (1,1,1) thin film is known to be self-limiting [36]. Due to the region between columnar structures shown in figure 2(d), oxygen and nickel-cation diffusion is likely enhanced, which is the case along grain boundaries and cracks [37]. An increased oxygen and nickel-cation diffusion rate would result in an increased oxidization of the surface, explaining the lack of MFM contrast.

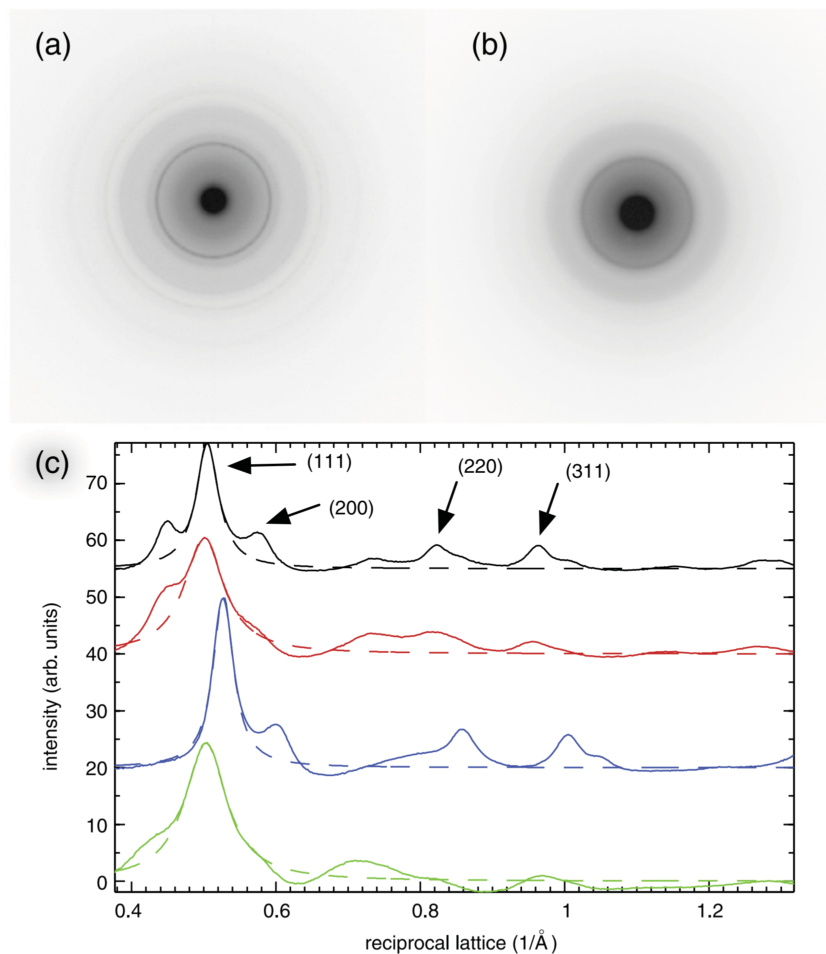

Figure 6. Selected area electron diffraction images of (a) the sample made using the PL stencil and (b) the sample made using the FIB-milled stencil. (c) Radially averaged with background subtracted of the sample made using the FIB-milled stencil (green), the sample made using the PL stencil (purple) and the FIB-milled stencil figure 2(e) zone 2 (red) and the FIB-milled stencil figure 2(e) zone 3 (black). Dashed lines represent fits to the (111) peaks. The peak at 0.45 $Å^{-1}$ is a result of the AuPd coating on the stencil.

4. Conclusion

SiN nanostencils milled using a FIB were shown to adversely influence the properties (film nanostructure, composition and magnetic behaviour) of permalloy nanostructures deposited by electron beam evaporation. The observed morphologies, chemical composition and magnetic behaviour were independent of the evaporator used and were repeated numerous times. We have attributed this effect to implanted gallium ions surrounding the milled nanostencil features which could provide a means for tunable control over the growth of magnetic nanostructures with varying iron content and film morphologies. This possible explanation does not account for the change in chemical composition and therefore more experiments are required to fully understand the resulting structures.

Acknowledgments

We thank Professors Mark Freeman, Professor John Davis, Dr Jessica Topple and Zaven Altounian for valuable discussions and Dr David Liu for TEM imaging. Funding from NSERC, FQRN, CIfAR and Alberta Innovates is gratefully acknowledged. FIB milling was performed at École Polytechnique de Montréal, electron beam evaporation was performed at the University of Alberta or at the McGill Nanotools Microfab, TEM was performed at the facility for electron microscopy research at McGill University and the EELS research described in this paper was performed at the Canadian Centre for Electron Microscopy at McMaster University, which is supported by NSERC and other government agencies.

References

[1] Chou S Y 1997 Patterned magnetic nanostructures and quantized magnetic disks *Proc. IEEE* **85** 652–71

[2] Martín J I, Nogués J, Liu K, Vicent J L and Schuller I K 2003 Ordered magnetic nanostructures: fabrication and properties *J. Magn. Magn. Mater.* **256** 449–501

[3] Ross C A, Smith H I, Savas T, Schattenburg M, Farhoud M, Hwang M, Walsh M, Abraham M C and Ram R J 1999 Fabrication of patterned media for high density magnetic storage *J. Vac. Sci. Technol.* B **17** 3168

[4] Deshmukh M M, Ralph D C C, Thomas M and Silcox J 1999 Nanofabrication using a stencil mask *Appl. Phys. Lett.* **75** 1631

[5] Brugger J, Berenschot J W, Kuiper S, Nijdam W, Otter B and Elwenspoek M 2000 Resistless patterning of sub-micron structures by evaporation through nanostencils *Microelectron. Eng.* **53** 403–5

[6] Vazquez-Mena O, Villanueva L G, Savu V, Sidler K, Langlet P and Brugger J 2009 Analysis of the blurring in stencil lithography *Nanotechnology* **20** 415303

[7] Linklater A and Nogami J 2008 Defining nanoscale metal features on an atomically clean silicon surface with a stencil *Nanotechnology* **19** 285302

[8] Fostner S, Burke S A, Topple J, Mativetsky J M, Beerens J and Grutter P 2010 Silicon nanostencils with integrated support structures *Microelectron. Eng.* **87** 652–7

[9] Kim G M, van den Boogaart M A F and Brugger J 2003 Fabrication and application of a full wafer size micro/nanostencil for multiple length-scale surface patterning *Microelectron. Eng.* **67/68** 609–14

[10] Egger S, Ilie A, Fu Y, Chongsathien J, Kang D-J and Welland M E 2005 Dynamic shadow mask technique: a universal tool for nanoscience *Nano Lett.* **5** 15–20

[11] Gross L, Schlittler R R, Meyer G, Vanhaverbeke A and Allenspach R 2007 Fabrication of ultrathin magnetic structures by nanostencil lithography in dynamic mode *Appl. Phys. Lett.* **90** 093121

[12] Zahl P, Bammerlin M, Meyer G and Schlittler R R 2005 All-in-one static and dynamic nanostencil atomic force microscopy/scanning tunneling microscopy system *Rev. Sci. Instrum.* **76** 023707

[13] Tsang W T and Cho A Y 1978 Molecular beam epitaxial writing of patterned GaAs epilayer structures *Appl. Phys. Lett.* **32** 491

[14] Gross L, Schlittler R R, Meyer G and Allenspach R 2010 Magnetologic devices fabricated by nanostencil lithography *Nanotechnology* **21** 325301

[15] Davis J P, Vick D, Li P, Portillo S K N, Fraser A E, Burgess J A J, Fortin D C, Hiebert W K and Freeman M R 2011 Nanomechanical torsional resonator torque magnetometry (invited) *J. Appl. Phys.* **109** 07D309

[16] Fraile Rodríguez A, Heyderman L J, Nolting F, Hoffmann A, Pearson J E, Doeswijk L M, van den Boogaart M A F and Brugger J 2006 Permalloy thin films exchange coupled to arrays of cobalt islands *Appl. Phys. Lett.* **89** 142508

[17] Joachim C, Martrou D, Rezeq M, Troadec C, Jie D, Chandrasekhar N and Gauthier S 2010 Multiple atomic scale solid surface interconnects for atom circuits and molecule logic gates. *J. Phys.: Condens. Matter* **22** 084025

[18] Guo H, Martrou D, Zambelli T, Polesel-Maris J, Piednoir A, Dujardin E, Gauthier S, van den Boogaart M A F, Doeswijk L M and Brugger J 2007 Nanostenciling for fabrication and interconnection of nanopatterns and microelectrodes *Appl. Phys. Lett.* **90** 093113

[19] Döehler G H, Hasnain G and Miller J N 1986 *In situ* grown-in selective contacts to n–i-p–i doping superlattice crystals using molecular beam epitaxial growth through a shadow mask *Appl. Phys. Lett.* **49** 704

[20] Tiggelaar R M, Berenschot J W, Elwenspoek M C, Gardeniers J G E, Dorsman R and Kleijn C R 2007 Spreading of thin-film metal patterns deposited on nonplanar surfaces using a shadow mask micromachined in Si(110) *J. Vac. Sci. Technol.* B **25** 1207

[21] Cojocaru C-V, Harnagea C, Rosei F, Pignolet A, van den Boogaart M A F and Brugger J 2005 Complex oxide nanostructures by pulsed laser deposition through nanostencils *Appl. Phys. Lett.* **86** 183107

[22] Tun T N, Lwin M H T, Kim H H, Chandrasekhar N and Joachim C 2007 Wetting studies on Au nanowires deposited through nanostencil masks *Nanotechnology* **18** 335301

[23] Köhler J, Albrecht M, Musil C R and Bucher E 1999 Direct growth of nanostructures by deposition through an Si_3N_4 shadow mask *Physica* E **4** 196–200

[24] Zhu X and Grutter P 2003 Magnetic force microscopy studies of patterned magnetic structures *IEEE Trans. Magn.* **39** 3420–5

[25] Grütter P, Rugar D and Mamin H J 1992 Magnetic force microscopy of magnetic materials *Ultramicroscopy* **47** 393–9

[26] Martin Y and Wickramasinghe H K 1987 Magnetic imaging by 'force microscopy' with 1000 Å resolution *Appl. Phys. Lett.* **50** 1455

[27] Egerton R F 2011 *Electron Energy-Loss Spectroscopy in the Electron Microscope* (Boston, MA: Springer)

[28] Bochkarev V F and Buchin E Yu 2009 The effect of electromagnetic fields on the process of formation of ultrathin Fe–Ni films during their deposition under a plasma-stimulated deposition *Russ. Microelectron.* **38** 165–70

[29] Rommel M, Spoldi G, Yanev V, Beuer S, Amon B, Jambreck J, Petersen S, Bauer A J and Frey L 2010 Comprehensive study of focused ion beam induced lateral damage in silicon by scanning probe microscopy techniques *J. Vac. Sci. Technol.* B **28** 595

[30] Spoldi G, Beuer S, Rommel M, Yanev V, Bauer A J and Ryssel H 2009 Experimental observation of FIB induced lateral damage on silicon samples *Microelectron. Eng.* **86** 548–51

[31] Fultz B and Howe J M 2008 *Transmission Electron Microscopy and Diffractometry of Materials* (Heidelberg: Springer)

[32] Mativetsky J M, Miyahara Y, Fostner S, Burke S A and Grutter P 2006 Use of an electron-beam evaporator for the creation of nanostructured pits in an insulating surface *Appl. Phys. Lett.* **88** 233121

[33] Jones T, Sawler J and Venus D 1993 Simple, calibrated deposition monitor incorporated into an electron beam evaporator *Rev. Sci. Instrum.* **64** 2008

[34] Nonnenmacher M, O'Boyle M P and Wickramasinghe H K 1991 Kelvin probe force microscopy *Appl. Phys. Lett.* **58** 2921

[35] Sadewasser S and Glatzel T (ed) 2012 *Kelvin Probe Force Microscopy* (*Springer Series in Surface Sciences*) vol 48 (Berlin: Springer)

[36] Ingo Flege J, Meyer A, Falta J and Krasovskii E E 2011 Self-limited oxide formation in Ni(111) oxidation *Phys. Rev.* B **84** 115441

[37] Atkinson H V 1985 A review of the role of short-circuit diffusion in the oxidation of nickel, chromium, and nickel-chromium alloys *Oxid. Met.* **24** 177–97